Materials Advances

ROYAL SOCIETY OF CHEMISTRY

PERSPECTIVE

View Article Online
View Journal | View Issue

Cite this: *Mater. Adv.*, 2022, 3, 6142

van der Waals epitaxy of transition metal dichalcogenides *via* molecular beam epitaxy: looking back and moving forward

Deependra Kumar Singh *[a] and Govind Gupta *[ab]

Received 28th March 2022,
Accepted 27th June 2022

DOI: 10.1039/d2ma00352j

rsc.li/materials-advances

Initiated by the discovery of graphene, tremendous research advances have been witnessed in the field of two-dimensional (2D) transition metal dichalcogenides (TMDCs) in the past few years. The unique optical and electrical properties of these layered TMDCs due to their well-defined low dimensionalities make them promising building blocks for next-generation electronics. Recently, a lot of research interest has been focussed on the growth of high-quality and large-area epilayers of several TMDCs using molecular beam epitaxy (MBE), owing to their ultra-high vacuum environment. The capability to precisely control the composition, thickness, and structural phases of TMDCs by MBE makes it suitable for studying fundamental sciences, investigating technological applications, and exploring new physics, which possibly could lead to fascinating applications. In the current perspective, an overview of the basic properties of TMDCs has been discussed, followed by the recent advancements in this area of the growth of TMDC thin films by MBE. Finally, the authors' viewpoints highlight this emerging research field's key challenges and opportunities.

1. Introduction

Over the last few decades, with the research advancements in the established and matured technology of traditional three-dimensional (3D) semiconductors such as III-nitrides, metal oxides, Si, *etc.*,[1–8] high-performance state-of-the-art electronic devices have been successfully fabricated. However, further progress and developments in these devices are often limited due to certain drawbacks encountered in these 3D semiconductors, for instance, the low charge carrier mobility, presence of dangling bonds at the surface, low light absorption properties, *etc.*[9,10] Hence, it becomes vital to explore alternatives that can overcome these limitations, for the development of next-generation devices. Therefore, two-dimensional (2D) layered materials have recently become a priority choice for applications in modern-day electronics.[11–15] The successful experimental realization of graphene[16] in 2004 led to a plethora of research in the field of ultrathin layered materials,[9,17–19] and several other graphene alternatives have been recently explored for various applications.[20–34] Among these, a particular class of layered materials, *i.e.*, transition metal dichalcogenides (TMDCs), has garnered significant interest, owing to their rich physics and fascinating potential applications.[35–41] TMDCs, just like graphene, can be scaled down to monolayers, although these TMDCs are three atoms thick instead of one.[42] TMDC-based devices possess considerable charge carrier mobility and a semiconducting band gap, making them suitable for switching applications,[25] and therefore, exhibit significant photoluminescence (PL) and intrinsic on-off current ratios as compared to graphene.[43–45] Additionally, TMDCs have also shown remarkable physical properties such as high tensile strength, making them a promising constituent in advanced device technology.[46]

However, the yield and cost are a major bottleneck in the extensive application of these layered materials. Presently, the most common and widely used technique to produce ultrathin TMDCs is exfoliation;[47–53] however, it presents specific common challenges such as the growth of high-quality thin films, scaling up for wafer-scale production, *etc.*[54,55] Therefore, considerable efforts have been made to research and optimize different production methodologies of these 2D layered TMDCs,[56–59] to improve their production yield without compromising the growth quality. One promising yet less-explored method to synthesize high-quality, epitaxial, and large area thin films of 2D TMDCs is *via* molecular beam epitaxy (MBE) due to its several potential advantages over the other growth techniques. The growth in MBE can be highly controlled because of the use of high-purity source materials, limiting contaminations due to growth carried out in an ultrahigh vacuum environment.[60–62]

Many reviews exist regarding the growth and applications of TMDCs by various synthesis techniques. McDonnell *et al.*[63]

[a] *Sensor Devices & Metrology Group, CSIR-National Physical Laboratory, Dr K. S. Krishnan Road, New Delhi – 110012, India. E-mail: deependras@iisc.ac.in*
[b] *Academy of Scientific & Innovative Research, CSIR-HRDC Campus, Ghaziabad, Uttar Pradesh – 201002, India. E-mail: govind@nplindia.org, govind.npl@nic.in*

have described the current status of TMDC thin film-based research, highlighting the importance of electronic and photonic applications. Lin *et al.*[64] have reported the recent progress in the field of thin-film synthesis and the processing techniques that exhibit excellent controllability and reliability for the substitutional doping of TMDC thin film monolayers. Walsh *et al.*[65] have discussed the various growth modes and the advantages of van der Waals (vdW) epitaxy, along with the most significant issues regarding the growth of TMDCs and topological insulators, including defect density, grain size control, electronic transport, doping, *etc.* Manzeli *et al.*[66] have examined the various synthesis methods for TMDCs along with a discussion about their properties, with specific focus on the superconductivity, charge density wave, and topological phases. Moreover, TMCD-based nanoelectronic devices have also been discussed and the strategies to improve and tailor the charge carrier properties have also been explored. However, a comprehensive analysis focussed on the recent advances and current prospects on TMDCs exclusively grown by MBE is still missing. In this perspective, we aim to provide a brief overview of MBE and the basic properties of TMDCs, following which an in-depth deliberation on the recent progress of the MBE-grown TMDCs for various applications is presented. Finally, we have discussed the unresolved issues and future perspectives for this evolving family of materials.

2. Transition metal dichalcogenides

TMDCs are represented by the formula MX_2, where M is a d block metal (Mo, W, Pd, Ti, *etc.*), and X represents a chalcogen (S, Te, and Se), respectively. The groups IV–X in the periodic table usually belong to these transition metals, containing a different number of valence d-electrons, giving rise to different electronic properties of these elements such as metallic, superconducting, semiconducting, *etc.*[66] TMDCs exist in a layered structure at the atomic level, consisting of one or a few monolayers.[67] A representative schematic depicting the layered structure of MoS_2 is shown in Fig. 1(a). TMDCs usually occur in several crystal structures due to the difference in the coordination environments of the transition metal. The two most common crystal structures of the TMDCs are the trigonal prismatic structure (2H) and the octahedral phase (1T). One can understand these structural phases in terms of the different stacking arrangements of the constituent atoms. Fig. 1(b) shows the different atomic structures of MoS_2. The three atoms, *i.e.*, chalcogen–transition metal–chalcogen, form the individual monolayers of TMDCs. The ABA stacking characterizes the 2H crystal phase, while the 1T octahedral phase corresponds to the ABC stacking sequence. Most of the TMDCs (MoS_2, WS_2, WSe_2, $MoSe_2$, $MoTe_2$, *etc.*) are thermodynamically more stable in their 2H phase than the metastable 1T octahedral phase.[67] In the 2H phase, TMDCs show semiconducting characteristics that accentuate TMDCs for potential next-generation electronic applications. The metastable or intermediate state for the 2H phase of TMDCs is the orthorhombic phase (1T′ phase). For WTe_2, the most stable crystal phase is the 1T′ phase at room temperature.[67]

Through the persevering efforts of researchers over the past few years, various techniques have been evolved to produce atomically ultrathin TMDCs.[9,10] In general, these synthesis techniques can be classified into two groups: the first method, known as the top-down technique, produces TMDC flakes by

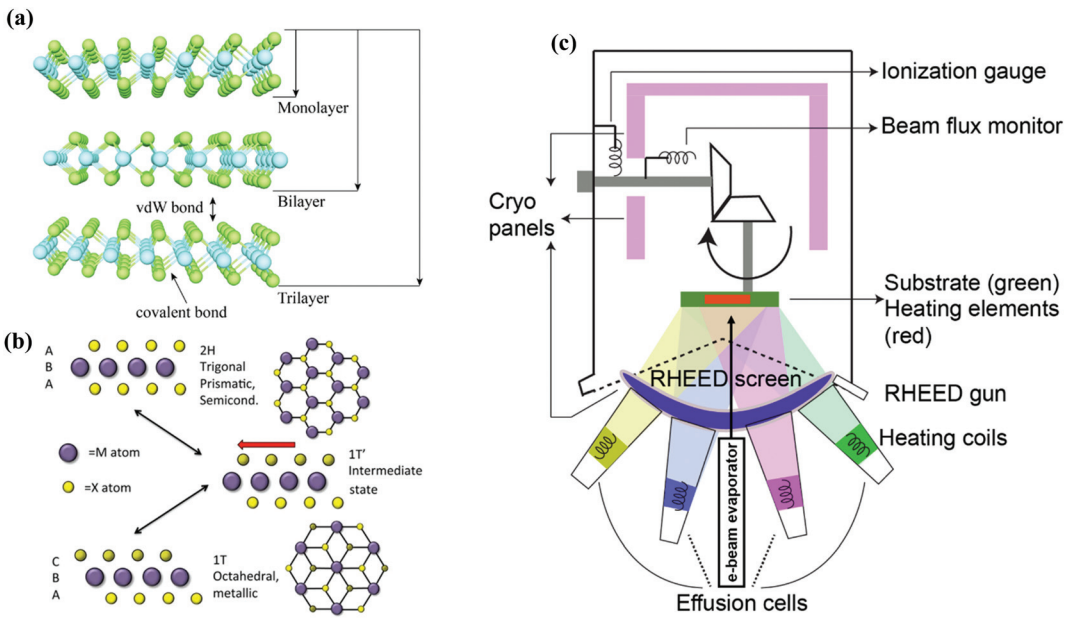

Fig. 1 (a) Schematic depicting multiple layers of MoS_2. Atoms of Mo are bonded *via* covalent bonds with S atoms. The individual layers are stacked together and held by weak vdW forces to form multi-layered or bulk structures. The figure has been reproduced from ref. 10. (b) Different crystal structures of MX_2, showing different stacking sequences. The two most common phases 2H and 1T, as well as the intermediate 1T′ phase, are shown. The figure has been reproduced from ref. 75. (c) Schematic diagram showing the various components of an MBE system. The figure has been adapted and reproduced from ref. 62.

thinning their bulk crystals. Different kinds of exfoliations fall in this group.[9,54,68,69] Since different monolayers of 2D TMDCs are held together by weak inter-layer vdW forces, under external perturbation, bulk 2D TMDC crystals readily get reduced into their few-layered flakes. The second approach is to grow layered TMDCs *via* bottom-up techniques, wherein the constituent species assemble to form continuous thin films. The main techniques under this category are atomic layer deposition,[70] magnetron sputtering,[71] chemical vapor deposition (CVD),[42,56] pulsed laser deposition (PLD),[36] and MBE.[72]

Among these methods, MBE is a very promising synthesis technique used to grow epitaxial thin films and heterostructures, where fine control over the layer thickness and ultra-high purity of the material components are required.[73,74] MBE involves the production of molecular/atomic beams of constituent source materials and/or doping species, which then react on the surface of a substrate to form an ordered thin film in an ultrahigh vacuum environment. The composition of this epitaxial thin film and its doping (if any) depends upon the arrival rate of the molecules/atoms and dopants, respectively. A typical MBE system consists of a stainless-steel ultrahigh vacuum chamber and various components such as vacuum pumps, substrate heater, effusion cells, *etc.* The source materials, usually of ultra-high purity (99.99%), are kept inside effusion cells (known as the Knudsen cells or K-cells). In the case of TMDCs, the transition metals are generally supplied from an e-beam evaporator, while the chalcogenides are placed inside these Knudsen cells.[72] Appropriate substrates are heated to the desired growth temperature and usually rotated to improve the uniformity and homogeneity of the final product. These Knudsen cells are then heated to high temperatures, depending on the required growth rates, the composition of the product, and the doping concentrations. The schematic of a typical MBE system is shown in Fig. 1(c), depicting the different components and the three zones where various physical phenomena occur. The details of the various processes in these zones have been described elsewhere.[62] The usual growth rates in an MBE process are a few hundred nm h^{-1} in contrast with other techniques where the growth rates are in the range of mm h^{-1}, thereby allowing the grown interfaces to be precisely controlled in their compositions. In addition, due to lower arrival rates of the species on the substrates, the growth is highly controlled along with the negligible probability of back-sputtering of the deposited film, which results into very smooth films with high control over the surface damage.

3. Recent advances in MBE-grown transition metal dichalcogenides

In this section, an overview is presented describing the recent progress in the field of MBE-grown TMDCs. Thin-film growth by MBE possesses the potential to isolate monolayers of TMDCs and synthesize large-area ultrathin films, which otherwise cannot be easily produced by exfoliation or other growth techniques. The growth of epitaxial TMDC films by MBE dates back to the mid-1980s.[76–78] These pioneering works have been done by Koma *et al.*[77] where they have demonstrated the growth of epitaxial $NbSe_2$ thin films, for the first time, on a cleaved 2H MoS_2 surface, following which, Koma *et al.*[78] successfully grew epitaxial $MoSe_2$ thin films on a $CaF_2(111)$ substrate. In both reports, the in-plane crystallographic axes of the grown thin films showed a high alignment towards the axes of the substrates used for their growth, despite the large lattice mismatches ($\sim$20%). Thus, the authors coined the term as ''vdW epitaxy,'' although extensive characterizations on the properties of these thin films were not carried out at that time. However, after almost three decades, recent research on different TMDCs has resurrected the concept of vdW epitaxy, and indeed there is an increasing number of research articles in this area being published in the last few years.[63–65,79] For instance, similar to the works carried out by Koma *et al.*,[77,78] Kreis *et al.*[80] have applied scanning tunnelling microscopy (STM) and angle-resolved photoemission spectroscopy (ARPES) to evaluate the electronic valence band spectra of HfS_2, during different stages of its epitaxial growth on WSe_2. In another report, Kreis *et al.*[81] have investigated the unoccupied and occupied electronic structures of HfS_2 ultrathin films, by employing combined angle-resolved photoemission and inverse photoemission, along with the band structure calculations. They have studied the impact of the thickness of the film on the two- and three-dimensional conduction and valence band states. Thus, a lot of research is being done in the field of MBE-grown TMDCs and in the coming subsections, the recent progress has been discussed.

3.1 Growth of selenides

In one of these early works, Barton *et al.*[82] have reported the growth of monolayer $HfSe_2$ on different substrates using MBE and have shown that this vdW epitaxy method allows the growth of high-quality heterostructures, without any strain or misfit dislocations in the thin films, in spite of the large lattice mismatch. Fig. 2(a) shows the high angle annular dark-field (HAADF) scanning transmission electron microscopy (STEM) image of $HfSe_2$ on MoS_2 grown by MBE. Peng *et al.*[83] have shown a nearly layer-by-layer growth of $TiSe_2$ ultrathin films on graphitized SiC(0001) substrate *via* MBE and have analyzed the defect structures of these films. The chemical inertness of graphene ensures a sharp interface between $TiSe_2$ thin films and SiC. The STM measurements reveal the identification of two dominant types of Se vacancies and interstitial defects (Fig. 2(b–d)).

Moreover, the observation of charge density waves (CDW) persisting down to monolayer $TiSe_2$, as shown in Fig. 2(e), favors the mechanism of the excitonic insulator in $TiSe_2$ thin films. These were a few early reports demonstrating the potential of the MBE as a growth technique for the production of TMDCs. In another report, Aretouli *et al.*[84] have shown the growth of high-quality vdW heterostructures of $SnSe_2/WSe_2$ by MBE on AlN/Si(111) substrates using Bi_2Se_3 as a buffer layer. 1T polytype of $SnSe_2$ is obtained having an indirect band gap of $\sim$0.8 eV with a strong and unintentionally doped n-type

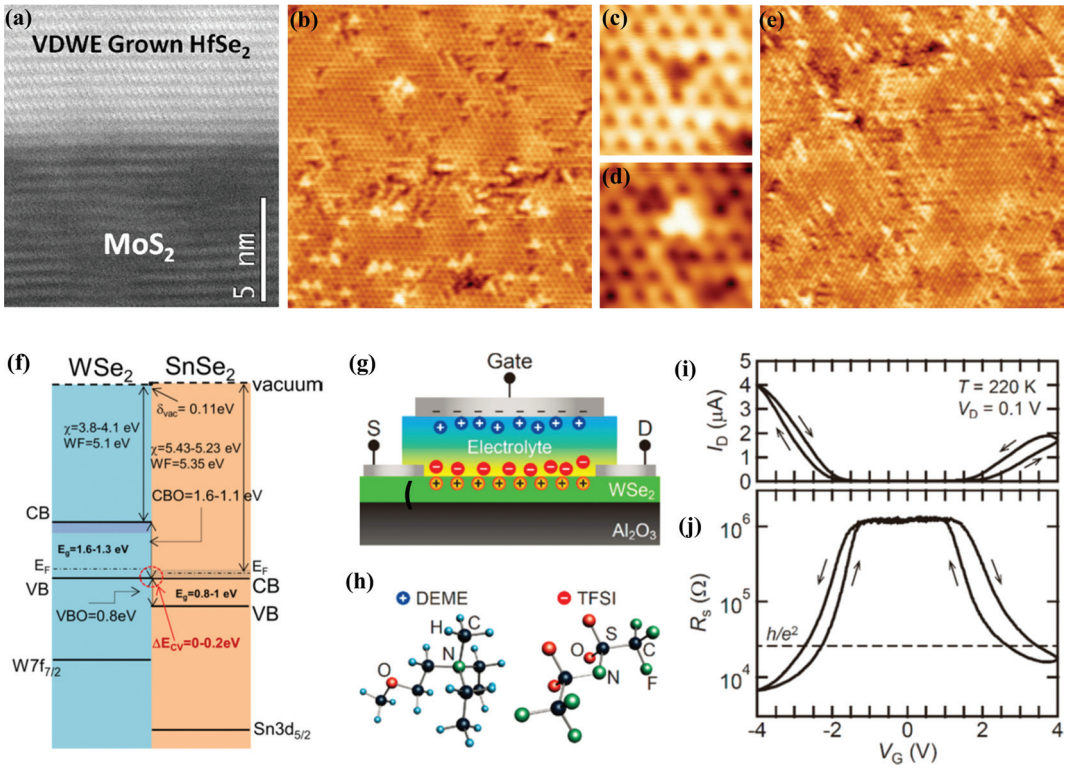

Fig. 2 (a) HAADF-STEM image of $HfSe_2$ grown on MoS_2 by MBE. The figure has been reproduced from ref. 82. (b) STM micrograph of $TiSe_2$ thin film (17 nm × 17 nm, I = 100 pA, and V_S = 0.24 V), showing the two kinds of Se defects: bright Se interstitials and dark Se vacancies. Zoomed-in STM micrographs of a single (c) Se vacancy and (d) interstitial (2 nm × 2 nm, I = 100 pA, and V_s = 0.24V). (e) STM micrograph of a charge density waves (CDW)-related 2 × 2 superstructure in single-layer $TiSe_2$ thin film (20 nm × 20 nm, I = 100 pA, and V_S = 0.1 V). The figures have been reproduced from ref. 83. (f) Schematic of the band alignment at the $WSe_2/SnSe_2$ heterojunction as revealed by X-ray photoelectron spectroscopy (XPS) core level analysis. E_F and χ denote the Fermi energy and electron affinity, respectively. E_g is the band gap, whereas VBO and CBO denote the valence and conduction band offsets, respectively. The figure has been reproduced from ref. 84. (g) Schematic of the top-gated electric-double-layer transistor (EDLT) based on the WSe_2 epitaxial thin film grown on the sapphire substrate. (h) Chemical structure of the electrolyte used in the electrolyte-gated transistor. (i and j) show typical transfer characteristics of WSe_2-EDLT carried out at T = 220 K, indicating clear ambipolar operation. The figures have been reproduced from ref. 79.

behavior. In contrast, the MBE-grown WSe_2 stabilizes in the 2H phase, exhibiting a p-type behavior. Band offsets analysis of this heterojunction revealed a nearly broken gap heterostructure as depicted in Fig. 2(f), which can be suitable for designing tunneling field-effect electronic devices. It must be noted that other groups have reported mid-gap or even slightly above mid-gap Fermi levels for MBE-grown epitaxial WSe_2 thin films, which correspond to an n-type behavior. For instance, Zhang *et al.*[85] have shown the successful synthesis of WSe_2 ultrathin films on an epitaxial bilayer graphene substrate with controlled film thickness at the atomic level. Employing *in situ* ARPES measurements, they have demonstrated the evolution of the electronic structure of the epitaxial WSe_2 thin films, which confirms a direct band gap for the single layer and bilayer WSe_2, and an indirect band gap for three or more layers of WSe_2. From the scanning tunnelling spectroscopic (STS) measurements, it is observed that an asymmetry exists between the valence band maximum and conduction band maximum, with respect to the Fermi level, revealing slightly n-type doping of the grown WSe_2 films. In another report, Blades *et al.*[86] have comprehensively studied the electronic and geometric structure of defects in WSe_2 thin films grown on highly oriented pyrolytic graphite (HOPG) with STS and STM, and the effect of temperature on the nature of these defects. In 2018, Wang *et al.*[87] reported the transport properties of highly crystalline epitaxial $TiSe_2$ thin films on a sapphire substrate grown by MBE. Robust CDW transitions have been demonstrated, down to 5 monolayers of $TiSe_2$ thin films, highlighting an exciting phenomenon of in-plane self-rotational growth of the epitaxial thin film with respect to the substrate. Yan *et al.*[88] have shown the successful growth of high-quality epitaxial $PtSe_2$ thin films with controlled thickness by MBE for the first time. In another work, Nakano *et al.*[79] have presented a study that demonstrates epitaxial and layer-by-layer growth of WSe_2 thin films on sapphire by MBE, utilizing an optimized growth recipe. They have also shown the ambipolar transistor operation of these thin films by an electrolyte gating technique (Fig. 2(g–j)). The enhancement in the drain current (I_D) is observed to be larger at the negative gate bias (V_G), which corresponds to the hole-doped regime compared to the positive gate voltages, corresponding to the electron-doped regime. Consequently, the four-probe sheet resistance (R_S) is found to be lower at the hole-doped side. The obtained results provide a benchmark towards the growth of epitaxial and large area TMDC thin films for

scalable devices. In a recent report by Freedy *et al.*,[89] the interfacial electrical resistance, interface chemistry, Seebeck coefficient, and thermal conductance of Ti, TiO_x, and Ti/TiO_x contacts to the MBE-grown WSe_2 thin films have been carried out. Metallic Ti exhibits a strong chemical reactivity with WSe_2 and results in W–Se bond scission, producing Ti–Se chemical states and metallic W. In addition, a high thermal boundary conductance along with low electrical resistance is also observed. On the other hand, TiO_x exhibits low reactivity, lower thermal boundary conductance, and higher electrical resistance. Due to the extremely small thermal conductance obtained and the Ohmic nature of the metal contacts, this interface may be promising for thermionic and thermoelectric applications. So, these works on MBE-grown TMDCs have shown promise to fabricate a variety of wafer-scale TMDC thin films and heterostructures in a carefully controlled manner, thereby, opening a route towards intensive fundamental and applied science research on TMDC-based structures.

One of the TMDCs that has been readily explored by MBE is $MoSe_2$.[90,91] Roy *et al.*[92] have reported the growth of $MoTe_2$ and $MoSe_2$ thin films on sapphire substrates and studied the temperature-dependent transport measurements of these thin films. The distinct layered structure of $MoTe_2$ thin films is apparent from the high-resolution cross-sectional transmission electron microscopy (HR-XTEM), along with the abrupt interface formed with the substrate, as shown in Fig. 3(a). The hexagonal lattice arrangement of the atoms has been shown in the plan-view TEM image in Fig. 3(b), and a lattice constant of 3.5 Å is extracted, which matches with that of bulk 2H $MoTe_2$. Fig. 3(c) shows the plan-view TEM micrograph of the $MoSe_2$ thin film, depicting a hexagonal lattice arrangement of atoms. The derived lattice constant of 3.3 Å is in good agreement with that of the bulk 2H $MoSe_2$. Moreover, an insulating behavior is observed for the grown thin films, which is in good agreement with 2D-variable range hopping (VRH), suggesting that the charge transport in these thin films is governed by the localized charge-carrier states (Fig. 3(d and e)). In another report, Chen *et al.*[72] have grown atomically thin, highly oriented, and ambipolar monolayer $MoSe_2$ on GaAs(111)B substrates. They have realized an electrolytically-gated transistor based upon the transferred $MoSe_2$ thin film (Fig. 3(f and g)), and it is perceived that the electrical transport characteristics of the device also follow the 2D-VRH (Fig. 3(h and i)) because of the disorders in the thin film. Ma *et al.*[93] have shown that twin grain boundaries in MBE-grown $MoSe_2$ thin films on different substrates are metallic in nature, substrate-independent, and undergo a Peierls metal to insulator transition at low temperatures. By utilizing STS measurements, substantial band gap narrowing of the $MoSe_2$ thin film is observed in the vicinity of these grain boundaries, which might be due to the stress induced within the film. It has been demonstrated in other reports that these twin boundaries in $MoSe_2$ have excess incorporation of Mo-atoms, which is a possible method for modifying $MoSe_2$ basal planes and consequently, altering their properties to potentially enhance their application in selective water adsorption.[94] Various other groups have also demonstrated the growth of $MoSe_2$ thin films on different 2D substrates, such as hexagonal boron nitride.[95] In a recent report, He *et al.*[96] have shown the gate-tuneable phonon properties of 2H $MoSe_2$ grown *via* MBE. The study demonstrates the electrostatically enhanced electron–phonon interactions in monolayer $MoSe_2$ thin films. It focuses on the correlation between the phonon properties and multiple valleys of monolayer and bilayer $MoSe_2$ thin films at different doping levels. The monolayer $MoSe_2$-based ion-gated devices also exhibit typical n-type transport characteristics with a high on/off ratio of $\sim 10^5$, along with a mobility of $\sim 31\ cm^2\ V^{-1}\ s^{-1}$.

Recently, Ohtake *et al.*[97] have successfully fabricated large-area 2D highly oriented $WSe_2/MoSe_2$ and $MoSe_2/WSe_2$ heterostructures using MBE, comprising consecutively stacked epitaxial WSe_2 and $MoSe_2$ monolayers on GaAs(111)B substrates, which have been pre-treated with Se. Fig. 3(j) displays the HAADF-STEM image of the MBE-grown bilayered $WSe_2/MoSe_2$ heterostructure, depicting the distinct layered structure. TMDC bilayered heterostructures can have several basic stacking geometries. In the most fundamental stacking geometry, the metal/chalcogen atoms of the first TMDC layer are on top of metal/chalcogen atoms of the second TMDC layer, where the T stacking geometry is obtained by the translation of the fundamental stacking sequence in such a way that the metal atoms of one of the TMDC layers are on top of the hexagonal centers of the other TMDC layer. In contrast, the C7 stacking geometry can be obtained from the T stacking *via* rotation of one TMDC layer concerning the other layer by an angle of 180° about the axis, which crosses a pair of overlapped chalcogen and metal atoms of the two TMDC layers (the metal atoms go on top of the chalcogen atoms and the chalcogen atoms go on top of the metal atoms).[98] The magnified image (shown on the right in Fig. 3(j)) confirms the formation of a C7-stacking configuration. In contrast, in the four-layered $MoSe_2/WSe_2$ heterostructure, as shown in Fig. 3(k), two kinds of stacking sequences, *i.e.*, C7 and T, are observed. The simultaneous formation of the T stacking configuration could be attributed to the small difference in the energies between the T and C7 stacking sequences for the $MoSe_2/WSe_2$ heterostructure. In other reports, wafer-scale growth of $MoSe_2$ has been achieved on a h-BN/sapphire substrate at a low growth temperature by combining the techniques of metal-organic vapor phase epitaxy (MOVPE) and MBE, revealing a large uniformity and homogeneity of the grown heterostructure on the whole wafer through an in-depth examination of the optical studies (Fig. 3(l–o)).[99] Recently, Wei *et al.*[100] have shown the complex nature of the nucleation and growth processes of $MoSe_2$ monolayers grown *via* MBE on mica. It has been observed that the 1T phase of $MoSe_2$ forms along with a comparable quantity of the 2H phase of $MoSe_2$, where the 1T phase converts gradually into the stable 2H phase before the complete growth of the first monolayer. These results demonstrate the possibility of stabilizing the metastable phases of atomically thin TMDCs by MBE.

3.2 Growth of sulfides

Recently, extensive research has also been focused on the growth of sulfides, such as MoS_2 thin films, utilizing MBE.

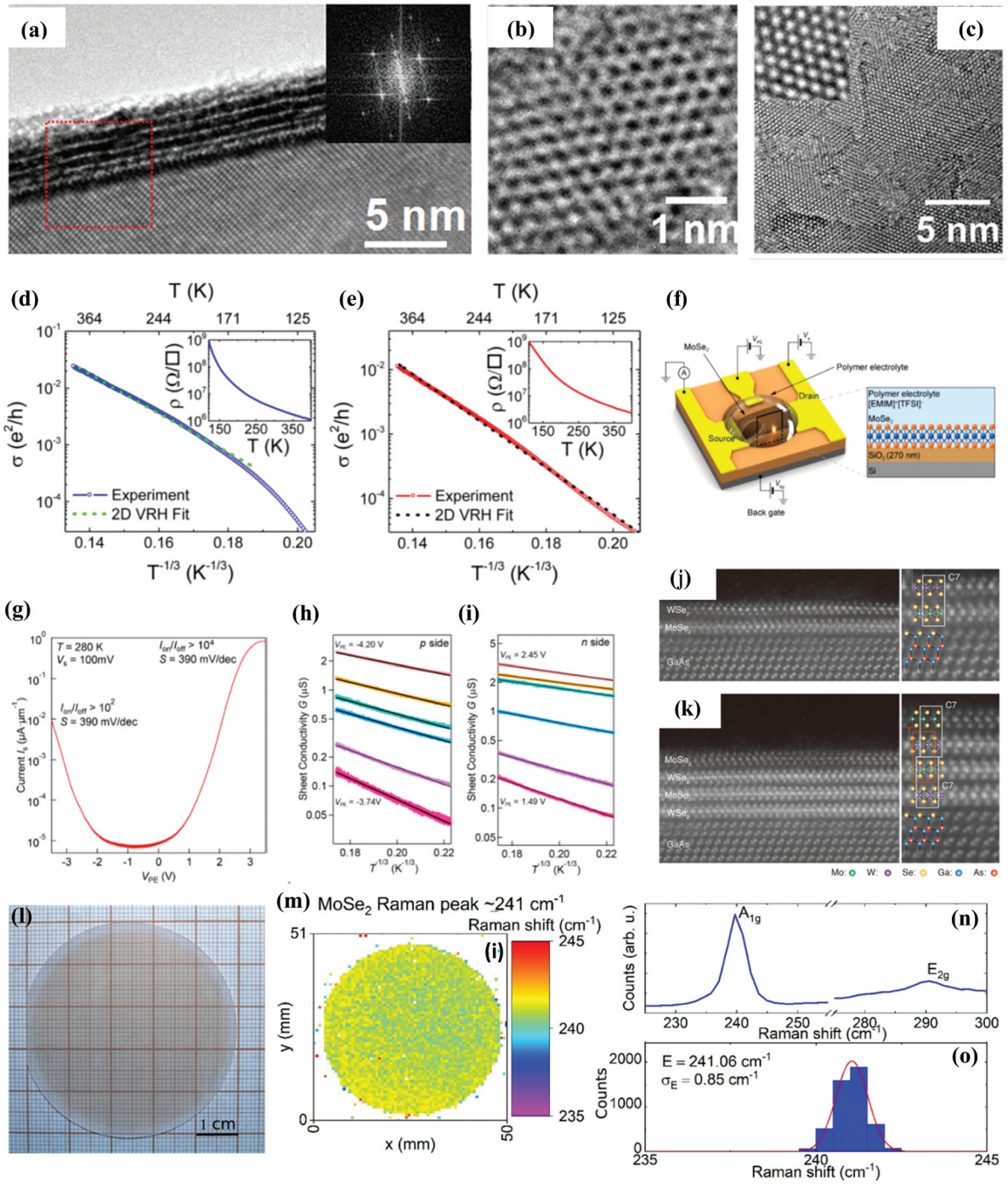

Fig. 3 (a) HR-XTEM image of a layered structure of $MoTe_2$. Inset shows the fast Fourier transform (FFT) of the area marked by the red square. The plan-view TEM image depicts the hexagonal arrangement of atoms in the (b) $MoTe_2$ thin film and (c) $MoSe_2$ lattice. Inset shows the zoomed-in view for 2×2 nm^2. Electrical transport measurements show the conductivity variation with $T^{-1/3}$ for (d) $MoTe_2$ and (e) $MoSe_2$. Insets of (d, e) show the variations of the measured resistivities with temperature. The figures have been reproduced from ref. 67. (f) The schematic device structure of the $MoSe_2$ thin film-based EDLT. (g) Variation of the channel current with polymer electrolyte voltage (VPE) depicting ambipolar behavior. (h and i) Sheet conductivity (G_{SH}) as a function of $T^{-1/3}$ on the p and n sides for different values of V_{PE}. The figure has been reproduced from ref. 45. The HAADF-STEM images for the (j) bilayered $WSe_2/MoSe_2$ and (k) four-layered $MoSe_2/WSe_2$ heterostructures grown on GaAs(111)B. The figure has been reproduced from ref. 71. (l) Optical image of epitaxially grown $MoSe_2$. (m) Peak energy of the A_{1g} mode obtained through Raman mapping. (n) Typical Raman spectrum of $MoSe_2$. (o) Distribution of the peak energy of the A1g mode indicating the mean value and standard deviation. The figure has been reproduced from ref. 73.

Fu *et al.*[101] have performed the growth of MoS_2 on h-BN under thermodynamically controlled conditions, which allow MoS_2 grains to align epitaxially on an h-BN substrate having the same orientation, thus, merging perfectly without the formation of

grain boundaries. In another report, El Kazzi *et al.*[102] have presented large-area growth of MoS_2 on 200 mm SiO_2/Si and Al_2O_3/Si templates using gas source MBE and have analysed the effect of the underneath surface template on the crystallinity of the MoS_2 layers. The HRTEM and HAADF-STEM images of MoS_2 on Al_2O_3/Si and MoS_2 on SiO_2/Si are shown in Fig. 4(a and b). The HRTEM images show the presence of a strong disorder in the MoS_2 thin film with clear crossing and overlapping of the atomic planes, which is because of the formation of small grains (~10 nm diameter). The energy dispersive spectroscopy (EDS) line profile shown in Fig. 4(b) reveals a small concentration of atomic Mo beneath the native oxide layer, indicating that Mo diffusion takes place through the thin native SiO_2 layer during the MoS_2 film deposition. On the other hand, this diffusion does not occur when an Al_2O_3 template is used (Fig. 4(a)), thereby efficiently blocking the diffusion of both Mo and S through the oxide layer. Xu *et al.*[103] have performed growth of 1H and 1T′ phases of nanosized MoS_2 islands on an Au(111) substrate by MBE and have analyzed the polymorph evolution by modulating the growth fluxes of Mo and S. A band gap opening of 80 meV at cryogenic temperatures (~4.5 K) for the 1T′ phase is noticed, which is in agreement with the predicted quantum spin Hall characteristics for the 1T′ phase of MoS_2. Fig. 4(c) shows the STS measurements of the 1T′ MoS_2 islands taken at the center, depicting a small band gap instead of the sharp V shape. The zoomed-in dI/dV curves taken at the edge and center of 1T′ islands are shown in Fig. 4(d), clearly indicating an energy gap opening of 75 ± 5 meV at the center. In another report, Ehlen *et al.*[104] have demonstrated the growth of epitaxial MoS_2 on a graphene/Ir(111) substrate and have reported a detailed spectroscopical analysis of this epitaxial system. A photoluminescence spectrum with a narrow peak width (~18 meV) has been observed. It was explained based on weak MoS_2–graphene interaction, preventing PL quenching, usually expected for metallic substrates. Mortelmans *et al.*[105] have studied the epitaxial growth of MoS_2 on sapphire and exfoliated MoS_2 flakes *via* MBE and MOVPE, and the analysis reveals that the technique of MBE yields superior epitaxial MoS_2 quality as compared with MOVPE. However, it was noticed that MBE provides greater control on the epitaxial registry in both cases. Recently, Ermolaev *et al.*[106] have presented a detailed study on the structural and optical properties of a monolayer of MoS_2 thin films grown by MBE on sapphire. The analysis has shown that the MBE-grown MoS_2 film exhibits a two-fold greater quantum yield of PL and lower photobleaching when compared with the CVD-synthesized MoS_2 films (Fig. 4(e)), thereby, making it a promising candidate for photonic applications.

3.3 Growth of tellurides

In addition, apart from the transition metal sulfides and selenides, researchers have also started exploring transition metal tellurides grown by MBE. Yu *et al.*[107] have reported the growth of continuous $MoTe_2$ thin films (atomically thin heterophase, homojunctions) across graphene substrates through MBE and have obtained the stoichiometric 2H and 1T′ phases of $MoTe_2$ simultaneously, showing potential for novel phase-patterning applications. The STS measurements performed on the thin films (from points A to G as shown in Fig. 5(a)) reveal

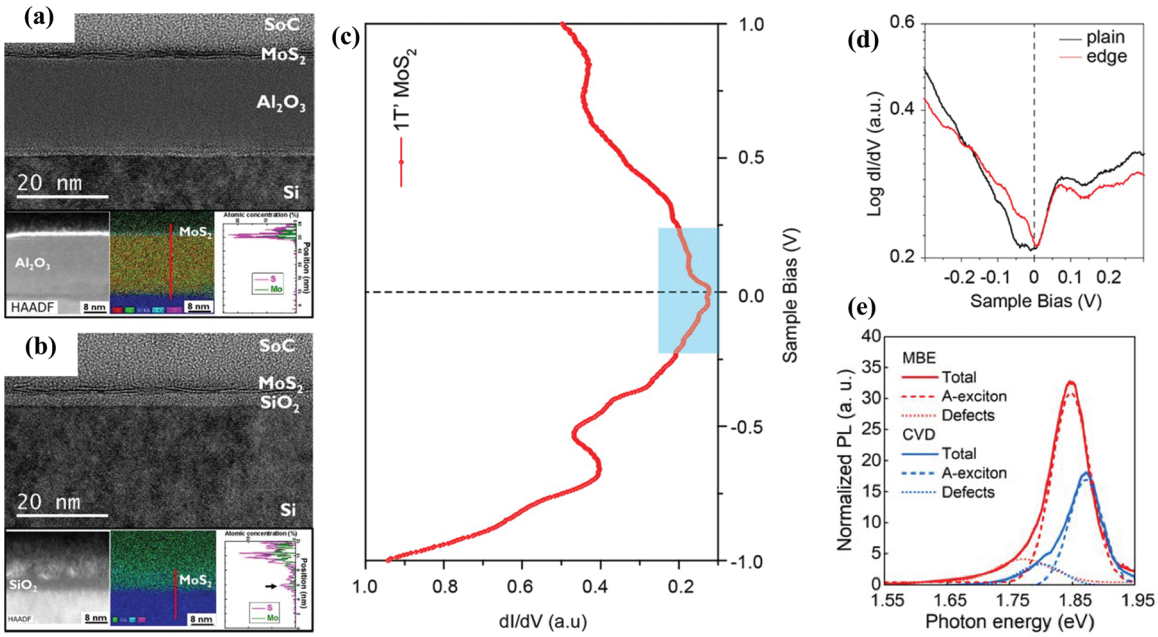

Fig. 4 The HR-TEM and HAADF-STEM images and the corresponding EDS mappings of (a) MoS_2 on Al_2O_3/Si and (b) MoS_2 on SiO_2/Si. The line profiles (red in color) in the EDS maps probe the concentrations of Mo and S atoms along the film/substrate interface. The figures have been reproduced from ref. 102. The electronic structure of the MBE-grown 1T′-MoS_2 nanocrystals at 4.5 K. (c) STS measurements taken at the bulk (center) of the 1T′-MoS_2 nanocrystals. (d) Zoomed-in views of the STS measurements of the 1T′-MoS_2 nanocrystals taken at the bulk and edge. The figure has been reproduced from ref. 103. (e) The PL spectra of the CVD and MBE-grown single-layer MoS_2 on Al_2O_3 substrates. Dotted and dashed lines indicate the deconvolution of the PL spectra into Gaussian peaks corresponding to defects and A-excitons, respectively. The figure has been reproduced from ref. 106.

"V"-type curves that gradually transform into "U"-type curves from point A to point G (differential conductance spectra shown in Fig. 5(b)). These results suggest the coherent phase transformation taking place from the semimetallic 1T′-$MoTe_2$ into the semiconducting 2H-$MoTe_2$. Walsh *et al.*[108] have reported the first-ever growth and characterization of WTe_2 thin films by MBE on several 2D substrates, including Bi_2Te_3, MoS_2, and graphite, and have enabled the growth of WTe_2 thin films in the distorted octahedral phase *via* interrupting the beam of the metal source. In another report, Li *et al.*[109] have discussed the growth of high-quality and epitaxial $PdTe_2$ thin film on a bilayer graphene/SiC(0001) substrate by MBE and have characterized this atomically thin film using STM. $PdTe_2$ has recently stimulated considerable research interest because of the underlying physics associated with this material system, as it exhibits the coexistence of both type-II Dirac fermions and superconductivity. ARPES measurements of a six-layered $PdTe_2$ thin film reveal a type-I Dirac cone contributing from Z2 topological surface states and their metallicity. Similarly, $PtTe_2$ is a type-II Dirac semimetal and exhibits unique photodetection capability in the mid infrared (MIR) region and robust ambient stability. Wei *et al.*[110] have recently shown large area and high-quality 1T-$PtTe_2$ monolayer thin films grown by MBE with excellent air stability. It is observed that a $PtTe_2$-based photodetector displays a photoresponse in a broad spectral range with high photoresponsivity and specific detectivity. The transmission electron microscopy (TEM) images of the grown $PtTe_2$ depict the hexagonal arrangement of the Pt and Te atoms with lattice spacings of 0.20 and 0.35 nm, corresponding to the (110) and (100) planes of the hexagonal phase of $PtTe_2$, respectively, as shown in Fig. 5(c–e). The $PtTe_2$-based photodetector shows a broadband photoresponse (bias voltage of 0.1 V) in the wavelength range of 420 nm–10.7 μm, exhibiting responsivities of 1.6 and 0.2 mA W^{-1} at 4.7 and 10.7 μm, respectively, as shown in Fig. 5(f and g). The three photoresponse cycles (Fig. 5(f)) maintain similar responsivities and noise levels, indicating stable and repeatable photodetection. In addition, these photodetectors also exhibit high sensitivity in the near infrared and visible regions.

Other transition metal di-tellurides to be successfully grown by MBE include monolayers of VTe_2, $TiTe_2$, and $CrTe_2$. In one such report, Lasek *et al.*[111] have shown that monolayer synthesis of

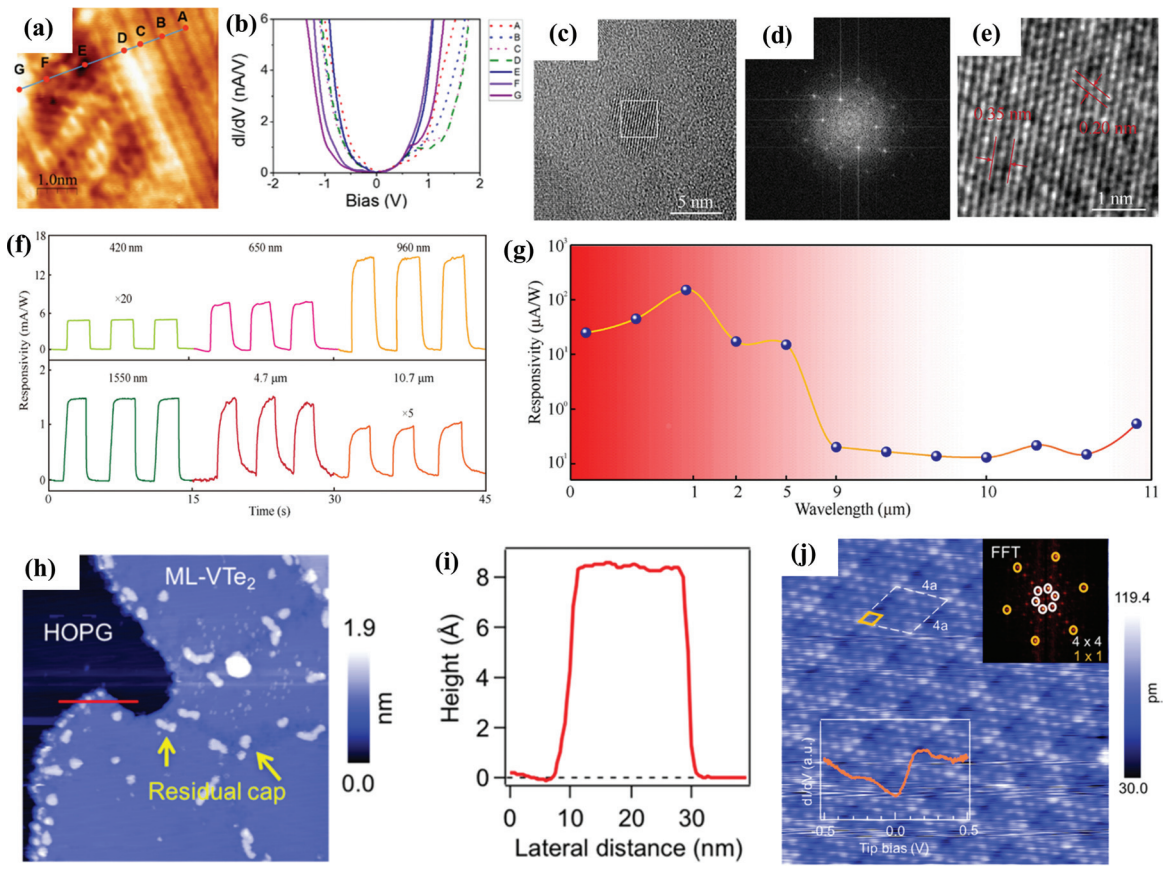

Fig. 5 (a) Atomic-resolution STM image (I_t = 300 pA, V_b = 500 mV) and the corresponding (b) STS curves of the 2H-1T′ $MoTe_2$/graphene ultrathin films. The figures have been reproduced from ref. 107. (c) The HRTEM image of the 1T-$PtTe_2$ thin film. (d) The zoomed-in image of the marked area in (c). (e) FFT of the layered 1T-$PtTe_2$ structure is shown in (d). (f) Spectral photoresponse of the $PtTe_2$. (g) Broadband photoresponse at different wavelengths (as indicated in the figure). The magnitudes of low responsivities (420 nm and 10.7 μm) have been multiplied for better visualization. The figure has been reproduced from ref. 110. (h) The STM image of monolayer VTe_2 measured at 77 K (150 × 150 nm^2; tunnelling current = 68 pA, tip bias = −0.89 V). Residual caps have been marked by yellow arrows. (i) A step height of ~8.5 Å indicates monolayer VTe_2 as shown in the line profile in (h). (j) The STM image showing atomic-resolution (10 × 10 nm^2; tunnelling current = 150 pA, tip bias = +0.1 V). The figure has been reproduced from ref. 112.

1T-TMDCs could be realized for all three early transition metal (Ti, V, and Cr) ditellurides *via* MBE, including the growth of $CrTe_2$, which is metastable only in its bulk form. In another report, Wong *et al.*[112] have presented direct spectroscopic and microscopic evidence of d^1 electronic configuration and metallic phase (1T) in monolayer VTe_2 grown by MBE on HOPG and a (4×4) CDW reconstruction pattern is obtained (Fig. 5(h–j)), different from the double zigzag chains observed in the bulk structure. Regarding the magnetic properties of the monolayer VTe_2, the X-ray magnetic circular dichroism (XMCD) measurements exclude the presence of an inherent ferromagnetic ordering, which contradicts the previous theoretical predictions.

3.4 Growth of chalcogenide-based alloys

Recently, 2D material-based alloys have also been investigated as they can represent a versatile platform that can extend the properties of the existing atomically thin TMDCs to the next level. Xie *et al.*[113] have realized the MBE growth of monolayer $Mo_xW_{1-x}Se_2$ alloys with controllable values of stoichiometric ratio. Utilizing *in situ* ARPES and XPS, the modifications in the valence band dispersion and the size of the spin-splitting have been determined by modulating the Mo/W ratios, as illustrated in Fig. 6(a–h). The growth of monolayers of these $Mo_xW_{1-x}Se_2$ alloys by MBE and the growth recipe for controlling the stoichiometric ratio paves an effective method for band structure engineering and spin-splitting in the 2D AB_2 family. Similarly, Zhang *et al.*[114] have investigated the synthesis of $V_xMo_{1-x}Se_2$ alloys by MBE on HOPG. A systematic study on the evolution of magnetism, electronic structure, and the thermal stability of $V_xMo_{1-x}Se_2$ alloys has been presented. Essentially, a critical value of x ($\sim$0.44) has been observed, above which the system remains as a homogeneous metallic phase and below which, separation of phases is favoured. Low vanadium concentrations ($x \leq \sim 0.05$) effectually increase the density of mirror twin boundaries in $MoSe_2$. Fig. 6(i–m) depict the evolution of the morphology of the 2D $V_xMo_{1-x}Se_2$ alloys and as the value of x increases, the crystalline domains gradually evolve from leaf-like ($MoSe_2$) into the triangular (VSe_2) form. The XMCD measurements show the absence of ferromagnetism down to 65 K, both in $V_xMo_{1-x}Se_2$ alloys and monolayer VSe_2. Thus, these works provide a comprehensive understanding of the electronic structures and properties of 2D TMDC alloys, which can be useful for designing futuristic 2D electronic devices.

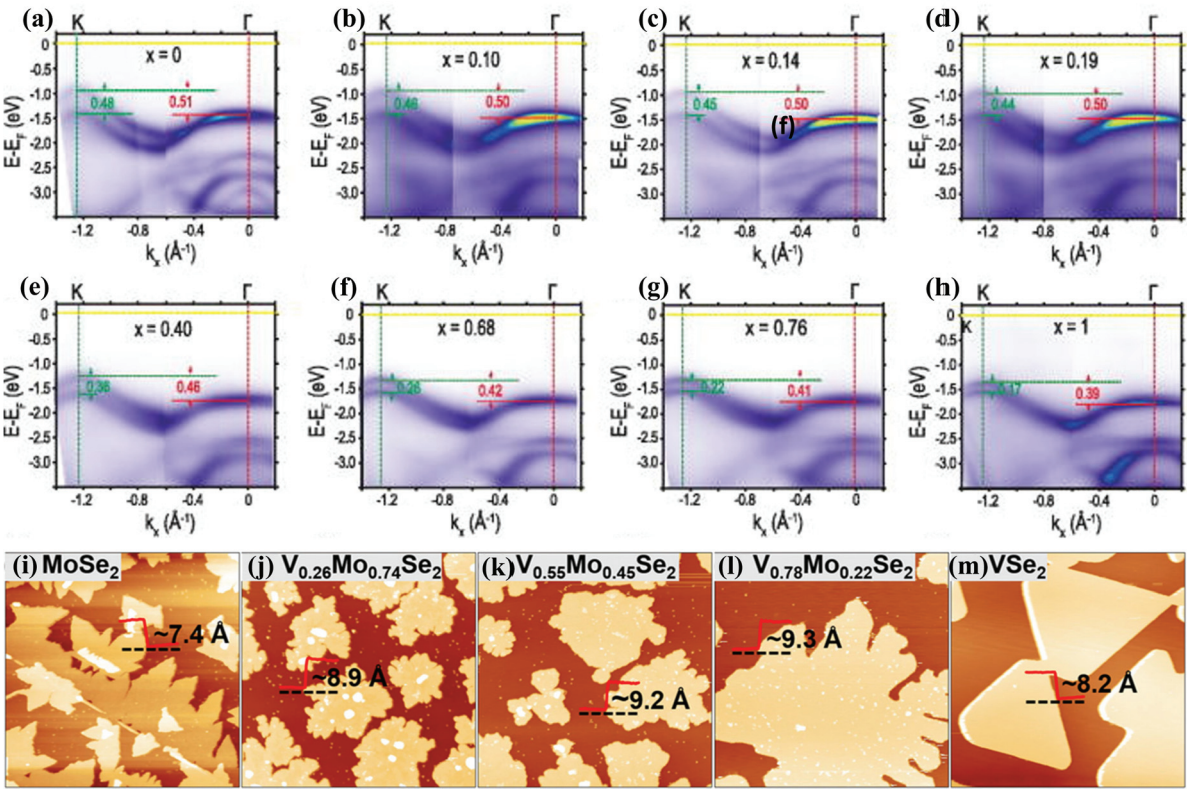

Fig. 6 The ARPES spectra of monolayer $Mo_xW_{1-x}Se_2$ thin films measured along the Γ–K direction with different Mo ratios (as indicated). The Mo ratios (x) in $Mo_xW_{1-x}Se_2$ from (a–h) can be stoichiometrically displayed as: (a) WSe_2, (b) $Mo_{0.10}W_{0.90}Se_2$, (c) $Mo_{0.14}W_{0.86}Se_2$, (d) $Mo_{0.19}W_{0.81}Se_2$, (e) $Mo_{0.40}W_{0.60}Se_2$, (f) $Mo_{0.68}W_{0.32}Se_2$, (g) $Mo_{0.76}W_{0.24}Se_2$, and (h) $MoSe_2$. The, green, yellow, and red lines indicate the energy levels at the K point, Fermi level, and C point, respectively. The energy difference between the K and Γ points, and the spin-splitting at the K point are also shown in (a–h). The figures have been reproduced from ref. 113. The STM and STS images of $V_xMo_{1-x}Se_2$ alloys (250 $\times$ 250 nm^2): (i) $MoSe_2$, (j) $V_{0.26}Mo_{0.74}Se_2$, (k) $V_{0.55}Mo_{0.45}Se_2$, (l) $V_{0.78}Mo_{0.22}Se_2$, and (m) VSe_2 (set points: (i) $-$3.8 V, 10 pA; (j) 1.6 V, 17 pA; (k) 1.6 V, 23 pA; (l) $-$1.6 V, 5 pA; (m) $-$0.5 V, 44 pA). The figure has been reproduced from ref. 114.

4. Summary and outlook

Recent years have witnessed remarkable progress in the MBE growth of a variety of TMDC thin films. In this article, we have discussed the fundamental properties of TMDCs, along with a brief review of the standard synthesis methods used for their fabrication. A short discussion on MBE has followed this, and finally, a progressive conversation regarding the MBE-growth of various TMDCs has been presented. These results unquestionably show the potential of MBE as one of the most promising and reliable techniques for the growth of high-quality TMDCs and contribute towards the advancement in the applications based on TMDCs in the future.

The published literature in this field indubitably indicates the substantial progress of TMDCs grown by MBE; however, the potential of this special class of materials still needs to be fully unearthed. Hence, a perspective and the associated follow-up research have been given below and illustrated in Fig. 7.

• The investigations on the MBE-fabricated TMDCs are still in the nascent phase, because of the recent popularity of MBE for the synthesis of TMDCs, in comparison to the other conventional synthesis techniques such as exfoliation and CVD. Thus, there still exists plenty of room for the enhancement of the crystal quality of these thin films by utilizing appropriate substrates for their growth and by further correlating the unexplored or much less explored growth parameters, for instance, the beam flux of the sources, annealing time, growth temperature, *etc.*[86,111,115–117]

• To date, most of the research in this field is limited to the growth of TMDC thin films and heterostructures. It is high time that focus needs to be given to fabricating MBE-grown TMDC-based devices, which can be promising in various applications such as photodetection, gas sensing, thermoelectrics, photocatalysis, energy generation, photovoltaics, *etc.*[89,118–121]

• Doping of MBE-grown TMDC thin films is another crucial area that needs to be explored in the future, which will help in enhancing the performance of TMDC-based devices. In addition, there is a great necessity to optimize p-type doping of TMDCs, which will be beneficial for the further growth of wide band gap n-type III-nitride semiconductors such as GaN or AlGaN to be utilized in p–n diodes, Esaki diodes, *etc.*[122–124]

• So far, promising results have been obtained in synthesizing semi-metallic phases of TMDCs (1T), which can be used in advanced optoelectronic applications, as they possess outstanding light absorption and electronic properties.[75,103,110,112,125–127]

• More research should be devoted to the study of TMDC-based alloys. Moreover, Janus TMDCs, which refer to transition metal layers with dissimilar surfaces, have engrossed intensive interest these days owing to their unique characteristics induced due to symmetry breaking and must be explored by MBE.[113,114,128]

• Even though the surfaces of TMDCs are more inert than those of non-layered materials, surface oxidation is still thermodynamically favored for TMDCs. Thus, the issue of surface oxidation needs to be solved and therefore, the study of the oxidation kinetics of the MBE-grown TMDCs can be an exciting area of investigation.[129,130]

As a concluding remark, MBE has emerged as a promising growth technique for large-scale TMDC thin films, and hence, holds the potential for use in next-generation device applications.

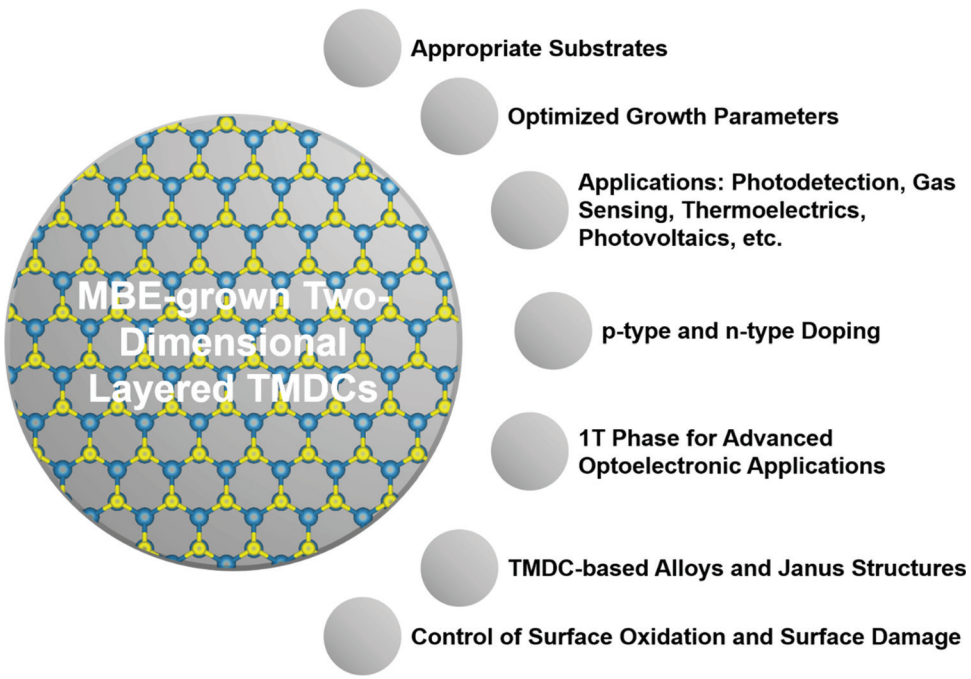

Fig. 7 Schematic illustrating the current prospects and opportunities to be explored in the field of MBE-grown TMDCs.

Conflicts of interest

The authors declare no conflicts of interest.

Acknowledgements

The authors would like to convey sincere gratitude to the Director, CSIR-NPL, New Delhi, India for his constant support. D. K. S. is thankful to the SERB National Postdoctoral Fellowship (PDF/2021/002469) for providing financial support.

References

1 W. Li, X. Zhang, R. Meng, J. Yan, J. Wang, J. Li and T. Wei, Epitaxy of III-nitrides on β-Ga_2O_3 and its vertical structure LEDs, *Micromachines*, 2019, **10**(5), 322.
2 N. Senthilkumar, E. Vivek, M. Shankar, M. Meena, M. Vimalan and I. V. Potheher, Synthesis of ZnO nanorods by one step microwave-assisted hydrothermal route for electronic device applications, *J. Mater. Sci.: Mater. Electron.*, 2018, **29**(4), 2927–2938.
3 M. Mukherjee and A. K. Singh, Strong chemical bond hierarchy leading to exceptionally high thermoelectric figure of merit in oxychalcogenide AgBiTeO, *ACS Appl. Mater. Interfaces*, 2020, **12**(7), 8280–8287.
4 A. Bapat, C. Anderson, C. R. Perrey, C. B. Carter, S. A. Campbell and U. Kortshagen, Plasma synthesis of single-crystal silicon nanoparticles for novel electronic device applications, *Plasma Phys. Control. Fusion*, 2004, **46**(12B), B97–B109.
5 H. S. Bae, M. H. Yoon, J. H. Kim and S. Im, Photodetecting properties of ZnO-based thin-film transistors, *Appl. Phys. Lett.*, 2003, **83**(25), 5313–5315.
6 J. Saroha, S. Mehra, M. Kumar and S. N. Sharma, Thermophysical properties of paraffin/TiO_2 and sorbitol/TiO_2 nanocomposites for enhanced phase change materials: a study on the stability issue, *Appl. Phys. A: Mater. Sci. Process.*, 2021, **127**(12), 916.
7 C. Pacholski, Photonic crystal sensors based on porous silicon, *Sensors*, 2013, **13**(4), 4694–4713.
8 A. M. Chowdhury, G. Chandan, R. Pant, B. Roul, D. K. Singh, K. K. Nanda and S. B. Krupanidhi, Self-powered, broad band, and ultrafast InGaN-based photodetector, *ACS Appl. Mater. Interfaces*, 2019, **11**(10), 10418–10425.
9 J. D. Yao, Z. Q. Zheng and G. W. Yang, Production of large-area 2D materials for high-performance photodetectors by pulsed-laser deposition, *Prog. Mater. Sci.*, 2019, **106**, 100573.
10 D. K. Singh, K. K. Nanda and S. B. Krupanidhi, Pulsed laser deposition of transition metal dichalcogenides-based heterostructures for efficient photodetection, in *Practical Applications of Laser Ablation*, ed. D. Yang, IntechOpen, London, 2021.
11 S. Das, A. Sebastian, E. Pop, C. J. McClellan, A. D. Franklin, T. Grasser, T. Knobloch, Y. Illarionov, A. V. Penumatcha, J. Appenzeller, Z. Chen, W. Zhu, I. Asselberghs, L.-J. Li, U. E. Avci, N. Bhat, T. D. Anthopoulos and R. Singh, Transistors based on two-dimensional materials for future integrated circuits, *Nat. Electron*, 2021, **4**(11), 786–799.
12 A. Sebastian, R. Pendurthi, T. H. Choudhury, J. M. Redwing and S. Das, Benchmarking monolayer MoS_2 and WS_2 field-effect transistors, *Nat. Commun.*, 2021, **12**(1), 693.
13 M. Mishra, A. Dash, A. Sharma, M. Khanuja and G. Gupta, CO sensing properties of nanostructured WSe_2/GaN and $MoSe_2$/GaN based gas sensors, *Phys. E*, 2022, 115147.
14 T. F. Schranghamer, M. Sharma, R. Singh and S. Das, Review and comparison of layer transfer methods for two-dimensional materials for emerging applications, *Chem. Soc. Rev.*, 2021, **50**(19), 11032–11054.
15 W. Zhu, T. Low, H. Wang, P. Ye and X. Duan, Nanoscale electronic devices based on transition metal dichalcogenides, *2D Mater.*, 2019, **6**(3), 032004.
16 K. S. Novoselov, A. K. Geim, S. V. Morozov, D. Jiang, Y. Zhang, S. V. Dubonos, I. V. Grigorieva and A. A. Firsov, Electric field effect in atomically thin carbon films, *Science*, 2004, **306**(5696), 666–669.
17 D. K. Singh, R. Pant, A. M. Chowdhury, B. Roul, K. K. Nanda and S. B. Krupanidhi, Defect-mediated transport in self-powered, broadband, and ultrafast photoresponse of a MoS_2/AlN/Si-based photodetector, *ACS Appl. Electron. Mater.*, 2020, **2**(4), 944–953.
18 A. Kumar, M. A. Khan and M. Kumar, Recent advances in UV photodetectors based on 2D materials: A review, *J. Phys. D: Appl. Phys.*, 2022, **55**(13), 133002.
19 M. A. Ribas, A. K. Singh, P. B. Sorokin and B. I. Yakobson, Patterning nanoroads and quantum dots on fluorinated graphene, *Nano Res.*, 2011, **4**(1), 143–152.
20 P. Li, C. Wang, J. Zhang, S. Chen, D. Guo, W. Ji and D. Zhong, Single-layer CrI3 grown by molecular beam epitaxy, *Sci. Bull.*, 2020, **65**(13), 1064–1071.
21 A. Rambabu, D. K. Singh, R. Pant, K. K. Nanda and S. B. Krupanidhi, Self-powered, ultrasensitive, room temperature humidity sensors using SnS_2 nanofilms, *Sci. Rep.*, 2020, **10**(1), 14611.
22 N. Goel and M. Kumar, 2D materials for terahertz application, *Nano Ex*, 2021, **2**(3), 031001.
23 P. Kumbhakar, C. Chowde Gowda, P. L. Mahapatra, M. Mukherjee, K. D. Malviya, M. Chaker, A. Chandra, B. Lahiri, P. M. Ajayan, D. Jariwala, A. Singh and C. S. Tiwary, Emerging 2D metal oxides and their applications, *Mater. Today*, 2021, **45**, 142–168.
24 P. Kumbhakar, M. Mukherjee, A. Pramanik, S. Karmakar, A. K. Singh, C. S. Tiwary and P. Kumbhakar, Confinement aided simultanous water cleaning and energy harvesting using atomically thin Wurtzite (Wurtzene), *Adv. Sustain. Syst*, 2021, **5**(2), 2000189.
25 D. K. Singh, R. Pant, B. Roul, A. M. Chowdhury, K. K. Nanda and S. B. Krupanidhi, Temperature-dependent electrical transport and optoelectronic properties of SnS_2/p-Si heterojunction, *ACS Appl. Electron. Mater*, 2020, **2**(7), 2155–2163.
26 T. Niu, New properties with old materials: Layered black phosphorous, *Nano Today*, 2017, **12**, 7–9.

27 Y. Li, H. Wang, L. Xie, Y. Liang, G. Hong and H. Dai, MoS_2 nanoparticles grown on graphene: An advanced catalyst for the hydrogen evolution reaction, *J. Am. Chem. Soc.*, 2011, **133**(19), 7296–7299.
28 R. Mas-Ballesté, C. Gómez-Navarro, J. Gómez-Herrero and F. Zamora, 2D materials: To graphene and beyond, *Nanoscale*, 2011, **3**(1), 20–30.
29 X. Zong, H. Yan, G. Wu, G. Ma, F. Wen, L. Wang and C. Li, Enhancement of photocatalytic H_2 evolution on CdS by loading MoS_2 as cocatalyst under visible light irradiation, *J. Am. Chem. Soc.*, 2008, **130**(23), 7176–7177.
30 K. Ellmer, Preparation routes based on magnetron sputtering for tungsten disulfide (WS_2) films for thin-film solar cells, *Phys. Status Solidi B*, 2008, **245**(9), 1745–1760.
31 D. Lembke, S. Bertolazzi and A. Kis, Single-layer MoS_2 electronics, *Acc. Chem. Res.*, 2015, **48**(1), 100–110.
32 A. P. Nayak, S. Bhattacharyya, J. Zhu, J. Liu, X. Wu, T. Pandey, C. Jin, A. K. Singh, D. Akinwande and J.-F. Lin, Pressure-induced semiconducting to metallic transition in multilayered molybdenum disulphide, *Nat. Commun.*, 2014, **5**(1), 3731.
33 N. Perea-López, A. L. Elías, A. Berkdemir, A. Castro-Beltran, H. R. Gutiérrez, S. Feng, R. Lv, T. Hayashi, F. López-Urías, S. Ghosh, B. Muchharla, S. Talapatra, H. Terrones and M. Terrones, Photosensor device based on few-layered WS_2 films, *Adv. Funct. Mater.*, 2013, **23**(44), 5511–5517.
34 X. Zong, J. Han, G. Ma, H. Yan, G. Wu and C. Li, Photocatalytic H_2 evolution on CdS loaded with WS_2 as cocatalyst under visible light irradiation, *J. Phys. Chem. C*, 2011, **115**(24), 12202–12208.
35 D.-H. Baek and J. Kim, MoS_2 gas sensor functionalized by Pd for the detection of hydrogen, *Sens. Actuators, B*, 2017, **250**, 686–691.
36 D. K. Singh, B. Roul, R. Pant, A. M. Chowdhury, K. K. Nanda and S. B. Krupanidhi, Different types of band alignment at MoS_2/(Al, Ga, In)N heterointerfaces, *Appl. Phys. Lett.*, 2020, **116**(25), 252102.
37 T. Roy, M. Tosun, X. Cao, H. Fang, D.-H. Lien, P. Zhao, Y.-Z. Chen, Y.-L. Chueh, J. Guo and A. Javey, Dual-gated MoS_2/WSe_2 van der Waals tunnel diodes and transistors, *ACS Nano*, 2015, **9**(2), 2071–2079.
38 D. K. Singh, R. K. Pant, K. K. Nanda and S. B. Krupanidhi, Differentiation of ultraviolet/visible photons from near infrared photons by MoS_2/GaN/Si-based photodetector, *Appl. Phys. Lett.*, 2021, **119**(12), 121102.
39 R. Yan, S. Fathipour, Y. Han, B. Song, S. Xiao, M. Li, N. Ma, V. Protasenko, D. A. Muller, D. Jena and H. G. Xing, Esaki diodes in van der Waals heterojunctions with broken-gap energy band alignment, *Nano Lett.*, 2015, **15**(9), 5791–5798.
40 S. K. Jain, M. X. Low, P. D. Taylor, S. A. Tawfik, M. J. S. Spencer, S. Kuriakose, A. Arash, C. Xu, S. Sriram, G. Gupta, M. Bhaskaran and S. Walia, 2D/3D hybrid of MoS_2/GaN for a high-performance broadband photodetector, *ACS Appl. Electron. Mater.*, 2021, **3**(5), 2407–2414.
41 S. K. Jain, R. R. Kumar, N. Aggarwal, P. Vashishtha, L. Goswami, S. Kuriakose, A. Pandey, M. Bhaskaran, S. Walia and G. Gupta, Current transport and band alignment study of MoS_2/GaN and MoS_2/AlGaN heterointerfaces for broadband photodetection application, *ACS Appl. Electron. Mater.*, 2020, **2**(3), 710–718.
42 S. L. Wong, H. Liu and D. Chi, Recent progress in chemical vapor deposition growth of two-dimensional transition metal dichalcogenides, *Prog. Cryst. Growth Charact. Mater.*, 2016, **62**(3), 9–28.
43 C.-H. Chen, C.-L. Wu, J. Pu, M.-H. Chiu, P. Kumar, T. Takenobu and L.-J. Li, Hole mobility enhancement and p-doping in monolayer WSe_2 by gold decoration, *2D Mater.*, 2014, **1**(3), 034001.
44 A. Splendiani, L. Sun, Y. Zhang, T. Li, J. Kim, C.-Y. Chim, G. Galli and F. Wang, Emerging photoluminescence in monolayer MoS_2, *Nano Lett.*, 2010, **10**(4), 1271–1275.
45 A. Yang, J. C. Blancon, W. Jiang, H. Zhang, J. Wong, E. Yan, Y. R. Lin, J. Crochet, M. G. Kanatzidis, D. Jariwala and T. Low, Giant enhancement of photoluminescence emission in WS_2-two-dimensional perovskite heterostructures, *Nano Lett.*, 2019, **19**(8), 4852–4860.
46 D. S. Schneider, A. Grundmann, A. Bablich, V. Passi, S. Kataria, H. Kalisch, M. Heuken, A. Vescan, D. Neumaier and M. C. Lemme, Highly responsive flexible photodetectors based on MOVPE grown uniform few-layer MoS_2, *ACS Photonics*, 2020, **7**(6), 1388–1395.
47 A. Raza, J. Z. Hassan, M. Ikram, S. Ali, U. Farooq, Q. Khan and M. Maqbool, Advances in liquid-phase and intercalation exfoliations of transition metal dichalcogenides to produce 2D framework, *Adv. Mater. Interfaces*, 2021, **8**(14), 2002205.
48 J. Y. Oh, J. H. Lee, S. W. Han, S. S. Chae, E. J. Bae, Y. H. Kang, W. J. Choi, S. Y. Cho, J.-O. Lee, H. K. Baik and T. I. Lee, Chemically exfoliated transition metal dichalcogenide nanosheet-based wearable thermoelectric generators, *Energy Environ. Sci.*, 2016, **9**(5), 1696–1705.
49 Q. H. Wang, K. Kalantar-Zadeh, A. Kis, J. N. Coleman and M. S. Strano, Electronics and optoelectronics of two-dimensional transition metal dichalcogenides, *Nat. Nanotechnol.*, 2012, **7**(11), 699–712.
50 H. Li, Y. Shi, M.-H. Chiu and L.-J. Li, Emerging energy applications of two-dimensional layered transition metal dichalcogenides, *Nano Energy*, 2015, **18**, 293–305.
51 S. B. Desai, S. R. Madhvapathy, M. Amani, D. Kiriya, M. Hettick, M. Tosun, Y. Zhou, M. Dubey, J. W. Ager, D. Chrzan and A. Javey, Gold-mediated exfoliation of ultralarge optoelectronically-perfect monolayers, *Adv. Mater.*, 2016, **28**(21), 4053–4058.
52 S.-S. Wu, T.-X. Huang, K.-Q. Lin, X. Yao, J.-T. Hu, D.-L. Tang, Y.-F. Bao and B. Ren, Photo-induced exfoliation of monolayer transition metal dichalcogenide semiconductors, *2D Mater.*, 2019, **6**(4), 045052.
53 A. Anto Jeffery, C. Nethravathi and M. Rajamathi, Two-dimensional nanosheets and layered hybrids of MoS_2 and WS_2 through exfoliation of ammoniated MS_2 (M = Mo, W), *J. Phys. Chem. C*, 2014, **118**(2), 1386–1396.
54 C.-Y. Huang, C. Chang, G.-Z. Lu, W.-C. Huang, C.-S. Huang, M.-L. Chen, T.-N. Lin, J.-L. Shen and T.-Y. Lin, Hybrid

2D/3D MoS_2/GaN heterostructures for dual functional photoresponse, *Appl. Phys. Lett.*, 2018, **112**(23), 233106.
55 C. Lee, H. Yan, L. E. Brus, T. F. Heinz, J. Hone and S. Ryu, Anomalous lattice vibrations of single- and few-layer MoS_2, *ACS Nano*, 2010, **4**(5), 2695–2700.
56 R. D. Nikam, P. A. Sonawane, R. Sankar and Y.-T. Chen, Epitaxial growth of vertically stacked P-MoS_2/n-MoS_2 heterostructures by chemical vapor deposition for light emitting devices, *Nano Energy*, 2017, **32**, 454–462.
57 M. I. Serna, S. H. Yoo, S. Moreno, Y. Xi, J. P. Oviedo, H. Choi, H. N. Alshareef, M. J. Kim, M. Minary-Jolandan and M. A. Quevedo-Lopez, Large-area deposition of MoS_2 by pulsed laser deposition with *in situ* thickness control, *ACS Nano*, 2016, **10**(6), 6054–6061.
58 T. A. J. Loh and D. H. C. Chua, Growth mechanism of pulsed laser fabricated few-layer MoS_2 on metal substrates, *ACS Appl. Mater. Interfaces*, 2014, **6**(18), 15966–15971.
59 L. Jiao, Y. Wang, Y. Zhi, W. Cui, Z. Chen, X. Zhang, W. Jie and Z. Wu, Fabrication and characterization of two-dimensional layered MoS_2 thin films by pulsed laser deposition, *Adv. Condens. Matter Phys.*, 2018, **2018**, 1–5.
60 I. Hernández-Rodríguez, J. M. García, J. A. Martín-Gago, P. L. de Andrés and J. Méndez, Graphene growth on Pt(111) and Au(111) using a MBE carbon solid-source, *Diam. Relat. Mater.*, 2015, **57**, 58–62.
61 J. M. J. Lopes, MBE growth of graphene, in *Molecular Beam Epitaxy*, John Wiley & Sons Ltd, Chichester, UK, 2019, pp. 395–409.
62 D. K. Singh, B. K. Roul, K. K. Nanda and S. B. Krupanidhi, Group III-nitrides and the C hybrid structures for next-generation photodetectors, in *Light-Emitting Diodes and Photodetectors – Advances and Future Directions*, ed. M. Casalino and J. Thirumalai, IntechOpen, London, 2021.
63 S. J. McDonnell and R. M. Wallace, Atomically-thin layered films for device applications based upon 2D TMDC materials, *Thin Solid Films*, 2016, **616**, 482–501.
64 Y. Lin, R. Torsi, D. B. Geohegan, J. A. Robinson and K. Xiao, Controllable thin-film approaches for doping and alloying transition metal dichalcogenides monolayers, *Adv. Sci.*, 2021, **8**(9), 2004249.
65 L. A. Walsh and C. L. Hinkle, van der Waals epitaxy: 2D materials and topological insulators, *Appl. Mater. Today*, 2017, **9**, 504–515.
66 S. Manzeli, D. Ovchinnikov, D. Pasquier, O. V. Yazyev and A. Kis, 2D transition metal dichalcogenides, *Nat. Rev. Mater.*, 2017, **2**(8), 17033.
67 M. Chhowalla, H. S. Shin, G. Eda, L.-J. Li, K. P. Loh and H. Zhang, The chemistry of two-dimensional layered transition metal dichalcogenide nanosheets, *Nat. Chem.*, 2013, **5**(4), 263–275.
68 A. Jawaid, D. Nepal, K. Park, M. Jespersen, A. Qualley, P. Mirau, L. F. Drummy and R. A. Vaia, Mechanism for liquid phase exfoliation of MoS_2, *Chem. Mater.*, 2016, **28**(1), 337–348.
69 G. Eda, H. Yamaguchi, D. Voiry, T. Fujita, M. Chen and M. Chhowalla, Photoluminescence from chemically exfoliated MoS_2, *Nano Lett.*, 2011, **11**(12), 5111–5116.
70 S. Balasubramanyam, M. J. M. Merkx, M. A. Verheijen, W. M. M. Kessels, A. J. M. Mackus and A. A. Bol, Area-selective atomic layer deposition of two-dimensional WS_2 nanolayers, *ACS Mater. Lett*, 2020, **2**(5), 511–518.
71 X. Mao, J. Zou, H. Li, Z. Song and S. He, Magnetron sputtering fabrication and photoelectric properties of WSe_2 film solar cell device, *Appl. Surf. Sci.*, 2018, **444**, 126–132.
72 M.-W. Chen, D. Ovchinnikov, S. Lazar, M. Pizzochero, M. B. Whitwick, A. Surrente, M. Baranowski, O. L. Sanchez, P. Gillet, P. Plochocka, O. V. Yazyev and A. Kis, Highly oriented atomically thin ambipolar $MoSe_2$ grown by molecular beam epitaxy, *ACS Nano*, 2017, **11**(6), 6355–6361.
73 N. Aggarwal, S. Krishna, S. Kumar Jain, M. Mishra, K. K. Maurya, S. Singh, M. Kaur and G. Gupta, Microstructural evolution of high quality AlN grown by PAMBE under different growth conditions, *Mater. Sci. Eng., B*, 2019, **243**, 71–77.
74 C. Ramesh, P. Tyagi, S. Gautam, S. Ojha, G. Gupta, M. S. Kumar and S. S. Kushvaha, Controlled growth of GaN nanorods directly on flexible Mo metal foil by laser molecular beam epitaxy, *Mater. Sci. Semicond. Process.*, 2020, **111**, 104988.
75 A. L. Friedman, A. T. Hanbicki, F. K. Perkins, G. G. Jernigan, J. C. Culbertson and P. M. Campbell, Evidence for chemical vapor induced 2H to 1T phase transition in MoX_2 (X = Se, S) transition metal dichalcogenide films, *Sci. Rep.*, 2017, **7**(1), 3836.
76 S. Tiefenbacher, H. Sehnert, C. Pettenkofer and W. Jaegermann, Epitaxial films of WS_2 by metal organic van der Waals epitaxy (MO-VDWE), *Surf. Sci.*, 1994, **318**(1–2), L1161.
77 A. Koma, K. Sunouchi and T. MiyaJima, Fabrication and characterization of heterostructures with subnanometer thickness, *Microelectron. Eng.*, 1984, **2**(1–3), 129–136.
78 A. Koma, K. Saiki and Y. Sato, Heteroepitaxy of a two-dimensional material on a three-dimensional material, *Appl. Surf. Sci.*, 1990, **41–42**, 451–456.
79 M. Nakano, Y. Wang, Y. Kashiwabara, H. Matsuoka and Y. Iwasa, Layer-by-layer epitaxial growth of scalable WSe_2 on sapphire by molecular beam epitaxy, *Nano Lett.*, 2017, **17**(9), 5595–5599.
80 C. Kreis, M. Traving, R. Adelung, L. Kipp and M. Skibowski, Tracing the valence band maximum during epitaxial growth of HfS_2 on WSe_2, *Appl. Surf. Sci.*, 2000, **166**(1–4), 17–22.
81 C. Kreis, S. Werth, R. Adelung, L. Kipp, M. Skibowski, E. E. Krasovskii and W. Schattke, Valence and conduction band states of HfS_2: From bulk to a single layer, *Phys. Rev. B*, 2003, **68**(23), 235331.
82 A. T. Barton, R. Yue, S. Anwar, H. Zhu, X. Peng, S. McDonnell, N. Lu, R. Addou, L. Colombo, M. J. Kim, R. M. Wallace and C. L. Hinkle, Transition metal dichalcogenide and hexagonal boron nitride heterostructures grown by molecular beam epitaxy, *Microelectron. Eng.*, 2015, **147**, 306–309.

83 J.-P. Peng, J.-Q. Guan, H.-M. Zhang, C.-L. Song, L. Wang, K. He, Q.-K. Xue and X.-C. Ma, Molecular beam epitaxy growth and scanning tunneling microscopy study of $TiSe_2$ ultrathin films, *Phys. Rev. B*, 2015, **91**(12), 121113.

84 K. E. Aretouli, D. Tsoutsou, P. Tsipas, J. Marquez-Velasco, S. Aminalragia Giamini, N. Kelaidis, V. Psycharis and A. Dimoulas, Epitaxial 2D $SnSe_2$/2D WSe_2 van der Waals heterostructures, *ACS Appl. Mater. Interfaces*, 2016, **8**(35), 23222–23229.

85 Y. Zhang, M. M. Ugeda, C. Jin, S.-F. Shi, A. J. Bradley, A. Martín-Recio, H. Ryu, J. Kim, S. Tang, Y. Kim, B. Zhou, C. Hwang, Y. Chen, F. Wang, M. F. Crommie, Z. Hussain, Z.-X. Shen and S.-K. Mo, Electronic structure, surface doping, and optical response in epitaxial WSe_2 thin films, *Nano Lett.*, 2016, **16**(4), 2485–2491.

86 W. H. Blades, N. J. Frady, P. M. Litwin, S. J. McDonnell and P. Reinke, Thermally induced defects on WSe_2, *J. Phys. Chem. C*, 2020, **124**(28), 15337–15346.

87 Y. Wang, M. Nakano, Y. Kashiwabara, H. Matsuoka and Y. Iwasa, Transport properties of a few nanometer-thick $TiSe_2$ films grown by molecular-beam epitaxy, *Appl. Phys. Lett.*, 2018, **113**(7), 073101.

88 M. Yan, E. Wang, X. Zhou, G. Zhang, H. Zhang, K. Zhang, W. Yao, N. Lu, S. Yang, S. Wu, T. Yoshikawa, K. Miyamoto, T. Okuda, Y. Wu, P. Yu, W. Duan and S. Zhou, High quality atomically thin $PtSe_2$ films grown by molecular beam epitaxy, *2D Mater.*, 2017, **4**(4), 045015.

89 K. M. Freedy, T. Zhu, D. H. Olson, P. M. Litwin, P. E. Hopkins, M. Zebarjadi and S. J. McDonnell, Interface chemistry and thermoelectric characterization of Ti and TiO_x contacts to MBE-grown WSe_2, *2D Mater.*, 2020, **7**(4), 045033.

90 S. Vishwanath, X. Liu, S. Rouvimov, P. C. Mende, A. Azcatl, S. McDonnell, R. M. Wallace, R. M. Feenstra, J. K. Furdyna, D. Jena and H. Grace Xing, Comprehensive structural and optical characterization of MBE grown $MoSe_2$ on graphite, CaF_2 and graphene, *2D Mater.*, 2015, **2**(2), 024007.

91 S. M. Poh, S. J. R. Tan, X. Zhao, Z. Chen, I. Abdelwahab, D. Fu, H. Xu, Y. Bao, W. Zhou and K. P. Loh, Large area synthesis of 1D-$MoSe_2$ using molecular beam epitaxy, *Adv. Mater.*, 2017, **29**(12), 1605641.

92 A. Roy, H. C. P. Movva, B. Satpati, K. Kim, R. Dey, A. Rai, T. Pramanik, S. Guchhait, E. Tutuc and S. K. Banerjee, Structural and electrical properties of $MoTe_2$ and $MoSe_2$ grown by molecular beam epitaxy, *ACS Appl. Mater. Interfaces*, 2016, **8**(11), 7396–7402.

93 Y. Ma, S. Kolekar, H. Coy Diaz, J. Aprojanz, I. Miccoli, C. Tegenkamp and M. Batzill, Metallic twin grain boundaries embedded in $MoSe_2$ monolayers grown by molecular beam epitaxy, *ACS Nano*, 2017, **11**(5), 5130–5139.

94 J. Li, T. Joseph, M. Ghorbani-Asl, S. Kolekar, A. V. Krasheninnikov and M. Batzill, Mirror twin boundaries in $MoSe_2$ monolayers as one dimensional nanotemplates for selective water adsorption, *Nanoscale*, 2021, **13**(2), 1038–1047.

95 S. M. Poh, X. Zhao, S. J. R. Tan, D. Fu, W. Fei, L. Chu, D. Jiadong, W. Zhou, S. J. Pennycook, A. H. Castro Neto and K. P. Loh, Molecular beam epitaxy of highly crystalline $MoSe_2$ on hexagonal boron nitride, *ACS Nano*, 2018, **12**(8), 7562–7570.

96 Z. He, T. Wei, W. Huang, W. Zhou, P. Hu, Z. Xie, H. Chen, S. Wu and S. Li, Electrostatically enhanced electron–phonon interaction in monolayer 2H-$MoSe_2$ grown by molecular beam epitaxy, *ACS Appl. Mater. Interfaces*, 2020, **12**(39), 44067–44073.

97 A. Ohtake and Y. Sakuma, Two-dimensional WSe_2/$MoSe_2$ heterostructures grown by molecular-beam epitaxy, *J. Phys. Chem. C*, 2021, **125**(20), 11257–11261.

98 F. Conte, D. Ninno and G. Cantele, Electronic properties and interlayer coupling of twisted MoS_2/$NbSe_2$ heterobilayers, *Phys. Rev. B*, 2019, **99**(15), 155429.

99 K. Ludwiczak, A. K. Dąbrowska, J. Binder, M. Tokarczyk, J. Iwański, B. Kurowska, J. Turczyński, G. Kowalski, R. Bożek, R. Stepniewski, W. Pacuski and A. Wysmołek, Heteroepitaxial growth of high optical quality, wafer-scale van der Waals heterostrucutres, *ACS Appl. Mater. Interfaces*, 2021, **13**(40), 47904–47911.

100 Y. Wei, C. Hu, Y. Li, X. Hu, K. Yu, L. Sun, M. Hohage and L. Sun, Initial stage of MBE growth of $MoSe_2$ monolayer, *Nanotechnology*, 2020, **31**(31), 315710.

101 D. Fu, X. Zhao, Y.-Y. Zhang, L. Li, H. Xu, A.-R. Jang, S. I. Yoon, P. Song, S. M. Poh, T. Ren, Z. Ding, W. Fu, T. J. Shin, H. S. Shin, S. T. Pantelides, W. Zhou and K. P. Loh, Molecular beam epitaxy of highly crystalline monolayer molybdenum disulfide on hexagonal boron nitride, *J. Am. Chem. Soc.*, 2017, **139**(27), 9392–9400.

102 S. El Kazzi, W. Mortelmans, T. Nuytten, J. Meersschaut, P. Carolan, L. Landeloos, T. Conard, I. Radu, M. Heyns and C. Merckling, MoS_2 synthesis by gas source MBE for transition metal dichalcogenides integration on large scale substrates, *J. Appl. Phys.*, 2018, **123**(13), 135702.

103 H. Xu, D. Han, Y. Bao, F. Cheng, Z. Ding, S. J. Tan and K. P. Loh, Observation of gap opening in 1T′ phase MoS_2 nanocrystals, *Nano Lett.*, 2018, **18**(8), 5085–5090.

104 N. Ehlen, J. Hall, B. V. Senkovskiy, M. Hell, J. Li, A. Herman, D. Smirnov, A. Fedorov, V. Yu Voroshnin, G. Di Santo, L. Petaccia, T. Michely and A. Grüneis, Narrow photoluminescence and Raman peaks of epitaxial MoS_2 on graphene/Ir(111), *2D Mater.*, 2018, **6**(1), 011006.

105 W. Mortelmans, S. El Kazzi, B. Groven, A. Nalin Mehta, Y. Balaji, S. De Gendt, M. Heyns and C. Merckling, Epitaxial registry and crystallinity of MoS_2 *via* molecular beam and metalorganic vapor phase van der Waals epitaxy, *Appl. Phys. Lett.*, 2020, **117**(3), 033101.

106 G. A. Ermolaev, M. A. El-Sayed, D. I. Yakubovsky, K. V. Voronin, R. I. Romanov, M. K. Tatmyshevskiy, N. V. Doroshina, A. B. Nemtsov, A. A. Voronov, S. M. Novikov, A. M. Markeev, G. I. Tselikov, A. A. Vyshnevyy, A. V. Arsenin and V. S. Volkov, Optical constants and structural properties of epitaxial MoS_2 monolayers, *Nanomaterials*, 2021, **11**(6), 1411.

107 Y. Yu, G. Wang, S. Qin, N. Wu, Z. Wang, K. He and X.-A. Zhang, Molecular beam epitaxy growth of atomically

ultrathin $MoTe_2$ lateral heterophase homojunctions on graphene substrates, *Carbon*, 2017, **115**, 526–531.

108 L. A. Walsh, R. Yue, Q. Wang, A. T. Barton, R. Addou, C. M. Smyth, H. Zhu, J. Kim, L. Colombo, M. J. Kim, R. M. Wallace and C. L. Hinkle, WTe_2 thin films grown by beam-interrupted molecular beam epitaxy, *2D Mater.*, 2017, **4**(2), 025044.

109 E. Li, R.-Z. Zhang, H. Li, C. Liu, G. Li, J.-O. Wang, T. Qian, H. Ding, Y.-Y. Zhang, S.-X. Du, X. Lin and H.-J. Gao, High quality $PdTe_2$ thin films grown by molecular beam epitaxy, *Chinese Phys. B*, 2018, **27**(8), 086804.

110 T. Wei, X. Wang, Q. Yang, Z. He, P. Yu, Z. Xie, H. Chen, S. Li and S. Wu, Mid-infrared photodetection of type-II Dirac semimetal 1T-$PtTe_2$ grown by molecular beam epitaxy, *ACS Appl. Mater. Interfaces*, 2021, **13**(19), 22757–22764.

111 K. Lasek, P. M. Coelho, K. Zberecki, Y. Xin, S. K. Kolekar, J. Li and M. Batzill, Molecular beam epitaxy of transition metal (Ti-, V-, and Cr-) tellurides: From monolayer ditellurides to multilayer self-intercalation compounds, *ACS Nano*, 2020, **14**(7), 8473–8484.

112 P. K. J. Wong, W. Zhang, J. Zhou, F. Bussolotti, X. Yin, L. Zhang, A. T. N'Diaye, S. A. Morton, W. Chen, J. Goh, M. P. de Jong, Y. P. Feng and A. T. S. Wee, Metallic 1T phase, 3d ^{1} electronic configuration and charge density wave order in molecular beam epitaxy grown monolayer vanadium ditelluride, *ACS Nano*, 2019, **13**(11), 12894–12900.

113 X. Xie, Y. Ding, J. Zong, W. Chen, J. Zou, H. Zhang, C. Wang and Y. Zhang, Band engineering in epitaxial monolayer transition metal dichalcogenides alloy $Mo_xW_{1-x}Se_2$ thin films, *Appl. Phys. Lett.*, 2020, **116**(19), 193101.

114 L. Zhang, T. Yang, X. He, W. Zhang, G. Vinai, C. S. Tang, X. Yin, P. Torelli, Y. P. Feng, P. K. J. Wong and A. T. S. Wee, Molecular beam epitaxy of two-dimensional vanadium-molybdenum diselenide alloys, *ACS Nano*, 2020, **14**(9), 11140–11149.

115 T. Jia, S. N. Rebec, S. Tang, K. Xu, H. M. Sohail, M. Hashimoto, D. Lu, R. G. Moore and Z.-X. Shen, Epitaxial growth of $TiSe_2/TiO_2$ heterostructure, *2D Mater.*, 2018, **6**(1), 011008.

116 P. M. Litwin, M. G. Sales, V. Nilsson, P. V. Balachandran, C. Constantin and S. McDonnell, The effect of growth temperature and metal-to-chalcogen on the growth of WSe_2 by molecular beam epitaxy, in *Low-Dimensional Materials and Devices 2019, vol. Proc. Spie 11085*, 2019, pp. 110850u.

117 A. Rajan, K. Underwood, F. Mazzola and P. D. C. King, Morphology control of epitaxial monolayer transition metal dichalcogenides, *Phys. Rev. Mater.*, 2020, **4**(1), 014003.

118 H. K. Sadhanala, S. Senapati, K. V. Harika, K. K. Nanda and A. Gedanken, Green synthesis of MoS_2 nanoflowers for efficient degradation of methylene blue and crystal violet dyes under natural sun light conditions, *New J. Chem.*, 2018, **42**(17), 14318–14324.

119 Y. Park, B. Ryu, S. J. Ki, B. McCracken, A. Pennington, K. R. Ward, X. Liang and K. Kurabayashi, Few-layer MoS_2 photodetector arrays for ultrasensitive on-chip enzymatic colorimetric analysis, *ACS Nano*, 2021, **15**(4), 7722–7734.

120 R. Bhandavat, L. David and G. Singh, Synthesis of surface-functionalized WS_2 nanosheets and performance as Li-ion battery anodes, *J. Phys. Chem. Lett.*, 2012, **3**(11), 1523–1530.

121 S. Dhara, H. Jawa, S. Ghosh, A. Varghese, D. Karmakar and S. Lodha, All-electrical high-sensitivity, low-power dual-mode gas sensing and recovery with a WSe_2/MoS_2 p–n heterodiode, *ACS Appl. Mater. Interfaces*, 2021, **13**(26), 30785–30796.

122 B. Wang, Y. Xia, J. Zhang, H.-P. Komsa, M. Xie, Y. Peng and C. Jin, Niobium doping induced mirror twin boundaries in MBE grown WSe_2 monolayers, *Nano Res.*, 2020, **13**(7), 1889–1896.

123 B. Tang, Z. G. Yu, L. Huang, J. Chai, S. L. Wong, J. Deng, W. Yang, H. Gong, S. Wang, K. W. Ang and Y. W. Zhang, Direct n to p-type channel conversion in monolayer/few-layer WS_2 field-effect transistors by atomic nitrogen treatment, *ACS Nano*, 2018, **12**(3), 2506–2513.

124 S. Krishnamoorthy, E. W. Lee, C. H. Lee, Y. Zhang, W. D. McCulloch, J. M. Johnson, J. Hwang, Y. Wu and S. Rajan, High current density 2D/3D MoS_2/GaN Esaki tunnel diodes, *Appl. Phys. Lett.*, 2016, **109**(18), 183505.

125 L. Cai, W. Cheng, T. Yao, Y. Huang, F. Tang, Q. Liu, W. Liu, Z. Sun, F. Hu, Y. Jiang, W. Yan and S. Wei, High-content metallic 1T phase in MoS_2-based electrocatalyst for efficient hydrogen evolution, *J. Phys. Chem. C*, 2017, **121**(28), 15071–15077.

126 M. Acerce, D. Voiry and M. Chhowalla, Metallic 1T phase MoS_2 nanosheets as supercapacitor electrode materials, *Nat. Nanotechnol.*, 2015, **10**(4), 313–318.

127 C. Xu, L. Jiang, X. Li, C. Li, C. Shao, P. Zuo, M. Liang, L. Qu and T. Cui, Miniaturized high-performance metallic 1T-phase MoS_2 micro-supercapacitors fabricated by temporally shaped femtosecond pulses, *Nano Energy*, 2020, **67**, 104260.

128 R. Sant, M. Gay, A. Marty, S. Lisi, R. Harrabi, C. Vergnaud, M. T. Dau, X. Weng, J. Coraux, N. Gauthier, O. Renault, G. Renaud and M. Jamet, Synthesis of epitaxial monolayer Janus SPtSe, *npj 2D Mater. Appl.*, 2020, **4**(1), 41.

129 P. M. Coelho, K. Lasek, K. Nguyen Cong, J. Li, W. Niu, W. Liu, I. I. Oleynik and M. Batzill, Monolayer modification of VTe_2 and its charge density wave, *J. Phys. Chem. Lett.*, 2019, **10**(17), 4987–4993.

130 M. G. Sales, S. T. Jaszewski, S. S. Fields, P. M. Litwin, J. F. Ihlefeld and S. J. McDonnell, Thermal stability of hafnium zirconium oxide on transition metal dichalcogenides, *Appl. Surf. Sci.*, 2021, **546**, 149058.